Junctional trafficking and restoration of retrograde signaling by the cytoplasmic RyR1 domain

Alexander Polster,[1] Stefano Perni,[1] Dilyana Filipova,[2] Ong Moua,[1] Joshua D. Ohrtman,[1] Hicham Bichraoui,[1] Kurt G. Beam,[1] and Symeon Papadopoulos[2]

[1]Department of Physiology and Biophysics, University of Colorado Denver Anschutz Medical Campus, Denver, CO
[2]Institute of Vegetative Physiology, University Hospital of Cologne, Cologne, Germany

The type 1 ryanodine receptor (RyR1) in skeletal muscle is a homotetrameric protein that releases Ca^{2+} from the sarcoplasmic reticulum (SR) in response to an "orthograde" signal from the dihydropyridine receptor (DHPR) in the plasma membrane (PM). Additionally, a "retrograde" signal from RyR1 increases the amplitude of the Ca^{2+} current produced by $Ca_V1.1$, the principle subunit of the DHPR. This bidirectional signaling is thought to depend on physical links, of unknown identity, between the DHPR and RyR1. Here, we investigate whether the isolated cytoplasmic domain of RyR1 can interact structurally or functionally with $Ca_V1.1$ by producing an N-terminal construct ($RyR1_{1:4300}$) that lacks the C-terminal membrane domain. In $Ca_V1.1$-null (dysgenic) myotubes, $RyR1_{1:4300}$ is diffusely distributed, but in RyR1-null (dyspedic) myotubes it localizes in puncta at SR–PM junctions containing endogenous $Ca_V1.1$. Fluorescence recovery after photobleaching indicates that diffuse $RyR1_{1:4300}$ is mobile, whereas resistance to being washed out with a large-bore micropipette indicates that the punctate $RyR1_{1:4300}$ stably associates with PM–SR junctions. Strikingly, expression of $RyR1_{1:4300}$ in dyspedic myotubes causes an increased amplitude, and slowed activation, of Ca^{2+} current through $Ca_V1.1$, which is almost identical to the effects of full-length RyR1. Fast protein liquid chromatography indicates that ~25% of $RyR1_{1:4300}$ in diluted cytosolic lysate of transfected tsA201 cells is present in complexes larger in size than the monomer, and intermolecular fluorescence resonance energy transfer implies that $RyR1_{1:4300}$ is significantly oligomerized within intact tsA201 cells and dyspedic myotubes. A large fraction of these oligomers may be homotetramers because freeze-fracture electron micrographs reveal that the frequency of particles arranged like DHPR tetrads is substantially increased by transfecting RyR-null myotubes with $RyR1_{1:4300}$. In summary, the RyR1 cytoplasmic domain, separated from its SR membrane anchor, retains a tendency toward oligomerization/tetramerization, binds to SR–PM junctions in myotubes only if $Ca_V1.1$ is also present and is fully functional in retrograde signaling to $Ca_V1.1$.

INTRODUCTION

Many cells transduce membrane depolarization into intracellular Ca^{2+} release, including skeletal muscle, where it is an essential step in excitation–contraction (EC) coupling. In skeletal muscle, the transduction occurs at triad junctions (Franzini-Armstrong, 1970) between t-tubules (plasma membrane [PM] invaginations) and the SR. Within the t-tubules, the dihydropyridine receptor (DHPR), which consists of a $Ca_V1.1$ subunit and auxiliary α_2-δ_1, β_{1a}, and γ_1 subunits, functions as the voltage-sensor for EC coupling and as a slowly activating, L-type Ca^{2+} channel. Because the entry of external Ca^{2+} is not required for skeletal-type EC coupling (Armstrong et al., 1972), it is widely thought that voltage-driven conformational changes of the DHPR that occur before L-type channel opening (Dirksen and Beam, 1999; Eltit et al., 2012) are mechanically coupled to the cytoplasmic domain of the type 1 RyR (RyR1), which in turn are conveyed to the RyR1 pore that spans the SR membrane, with the result that Ca^{2+} is released from the SR. Additionally, there is a retrograde interaction between RyR1 and the DHPR such that the presence of RyR1 substantially increases the amplitude of the L-type Ca^{2+} current produced by the DHPR (Nakai et al., 1996) and slows the current's activation (Avila and Dirksen, 2000). Identifying the sites of protein–protein interaction that underlie the bidirectional signaling interactions has been difficult to achieve for several reasons. Foremost, perhaps, is the large size of the RyR1 homotetramer: each monomer contains ~5,000 residues, of which only ~500 C-terminal residues are embedded in or associated with the SR membrane and contribute to the formation of the Ca^{2+} permeable pore (Du et al., 2002; Efremov et al., 2015; Yan et al., 2015; Zalk et al., 2015). Thus, most of the RyR1 homotetramer is cytoplasmic and is visible in electron micrographs as the "foot" structure spanning the ~12-nm gap between the SR and t-tubular membranes (Franzini-Armstrong, 1970).

A variety of evidence indicates that the DHPR and RyR1 are physically linked to one another, although

Correspondence to Symeon Papadopoulos: symeon.papadopoulos@uni-koeln.de

the identity of these links, and whether they are direct or indirect, remains unknown. In particular, freeze-fracture electron microscopy (EM) reveals that DHPRs are arrayed in groups of four (tetrads), such that each tetrad is aligned with the four, homomeric subunits of every other RyR1 in the junctional SR beneath them (Block et al., 1988). In dyspedic myotubes (null for RyR1), PM–SR junctions still form and the junctional domains of the PM contain DHPRs, but these are no longer arranged into tetrads; however, tetrads are restored by the expression of exogenous RyR1 (Protasi et al., 1998). Moreover, in wild-type muscle cells, the pharmacologically induced transition of RyR1 into an inactivated state causes an ∼2-nm decrease in the distance separating DHPRs within tetrads (Paolini et al., 2004a).

The targeting of full-length RyR1 to triad junctions, which does not depend on the presence of DHPRs (Franzini-Armstrong et al., 1991), causes RyR1 to be concentrated within the narrow gap separating the SR and t-tubular membranes, and this would be expected to stabilize interactions that occur between the cytoplasmic domain of RyR1 and the DHPR. Here, we have tested whether the RyR1 cytoplasmic domain, lacking the SR membrane-anchoring segments, can still physically link to DHPRs in junctional domains of the PM, and whether such binding alters the function and/or ultrastructural arrangement of the DHPRs. To do so, we constructed an expression plasmid encoding only the N-terminal 4,300 residues of RyR1 ($RyR1_{1:4300}$; ∼500 kD), which constitutes the bulk of the RyR1 cytoplasmic domain and lacks the 537 C-terminal residues that contain the transmembrane segments that anchor the protein in the SR membrane (Du et al., 2002). Based on the structures determined for the RyR1 homotetramer by cryo-EM (Efremov et al., 2015; Yan et al., 2015; Zalk et al., 2015), the $RyR1_{1:4300}$ sequence terminates in a region that lacks defined structure and is downstream of the last major cytoplasmic region of defined structure (termed either the "solenoid" or "central domain") and upstream of the membrane spanning α-helices and cytoplasmic C-terminal domain.

When expressed in dysgenic myotubes lacking the DHPR $Ca_V1.1$ subunit, $RyR1_{1:4300}$ displayed a diffuse cellular distribution. However, when the DHPR $Ca_V1.1$ subunit was present, $RyR1_{1:4300}$ accumulated at junctions, indicating $Ca_V1.1$-dependent interaction(s). Surprisingly, $RyR1_{1:4300}$ was equivalent to full-length RyR1 with respect to retrograde signaling to the DHPR. In particular, expression of either RyR1 or $RyR1_{1:4300}$ in dyspedic myotubes produced a similar increase in amplitude, and slowing of activation, of the L-type Ca^{2+} current. Fast protein liquid chromatography (FPLC) revealed that the majority of $RyR1_{1:4300}$ was monomeric in dilute cytosolic lysate of transfected tsA201 cells but that higher molecular weight complexes were also present. However,

at the higher concentrations prevailing within intact tsA201 cells and myotubes, intermonomer fluorescence resonance energy transfer (FRET) indicated $RyR1_{1:4300}$ was substantially oligomerized. Expression of $RyR1_{1:4300}$ in RyR-null myotubes caused the DHPRs to be arranged into tetrads, supporting the idea that an appreciable fraction of the oligomers was tetrameric.

MATERIALS AND METHODS

RyR1 constructs N-terminally tagged with enhanced fluorescent protein

As the starting point, the coding sequence for the full-length rabbit RyR1 (GenBank number X15209.1; Takeshima et al., 1989) was excised from the GFP-RyR1 plasmid described by Lorenzon et al. (2001) and transferred to modified versions of EXFP-C1 mammalian expression vectors (Clontech; EXFP referring to ECFP, EGFP, or EYFP). This required that the multiple cloning site (mcs) of EXFP-C1 be shifted to match the reading frame of the RyR1 insert. This shift was achieved by first removing the XhoI-SalI fragment from the mcs of EXFP-C1 and then replacing it with the flipped XhoI-SalI fragment of the EYFP-N1 mcs (Clontech; this is possible because XhoI and SalI cut ends are compatible with one another). A HindIII site, which resided within the flipped XhoI-SalI insert of the resulting plasmid ($EXFP-C1_{flip}$), was used for inserting the RyR1 coding sequence. To obtain this sequence, the GFP-RyR1 plasmid (Lorenzon et al., 2001) was cut with HindIII and KpnI, producing a short N-terminal HindIII-KpnI RyR1 fragment (875 bp) and a long C-terminal KpnI-KpnI RyR1 fragment (14,264 bp). The N-terminal RyR1 fragment was ligated into $EXFP-C1_{flip}$ mcs after digestion of the latter with HindIII and KpnI. Subsequently, the C-terminal RyR1 fragment was inserted into the KpnI site of the $EXFP-C1_{flip}$ plasmid, which already contained the N-terminal RyR1 fragment, with correct orientation confirmed by restriction analysis. The resulting plasmids (ECFP-RyR1, EGFP-RyR1, and EYFP-RyR1) were used to generate N-terminally tagged $RyR1_{1:4300}$ plasmids by digestion with SacII, which produced three DNA fragments (10,396 bp, 7,217 bp, and 2,238 bp). The two larger DNA fragments, containing the sequences encoding $RyR1_{1:4300}$ and the vector backbone, were ligated to generate $ECFP-RyR1_{1:4300}$, $EGFP-RyR1_{1:4300}$, and $EYFP-RyR1_{1:4300}$.

Cell culture and cDNA transfection

Primary myoblasts were harvested (Beam and Franzini-Armstrong, 1997) from newborn mice that were dysgenic (homozygous for absence of the DHPR $Ca_V1.1$ subunit; Tanabe et al., 1988), dyspedic (homozygous for absence of RyR1; Buck et al., 1997), or homozygous null for both $Ca_V1.1$ and RyR1, which were obtained by crossbreeding of heterozygous dysgenic and dyspedic

mice (absence of both transcripts confirmed by PCR). The myoblasts were maintained for 4–5 d after plating in a humidified 37°C incubator with 5% CO_2 in Dulbecco's Modified Eagle Medium (DMEM; Mediatech), supplemented with 10% FBS/10% horse serum (Hyclone Laboratories). This medium was then replaced with differentiation medium (DMEM supplemented with 2% horse serum). Immortalized, RyR1-RyR3 double-null myoblasts (R1R3; Moore et al., 1998) were also used. For electrophysiological experiments, the myoblasts were plated into 35-mm enhanced chemiluminescence (ECL)-coated (Merck Millipore), plastic culture dishes (Falcon) and for imaging and freeze-fracture were plated onto 35-mm dishes with ECL-coated glass coverslip bottoms (MatTek). R1R3 myoblasts were kept for 2 d after plating (at 5×10^3 in the center of glass coverslip-bottom dishes) in Ham's F-10 Nutrient Mixture (Life Technologies Inc.), supplemented with 20% bovine serum (Hyclone Laboratories), and then switched to R1R3 differentiation medium: low glucose DMEM (Life Technologies, Inc.) supplemented with 2% horse serum. Either 2–4 d (primary myotubes) or 3 d (R1R3 myotubes) after switching to differentiation medium, single nuclei were injected with plasmid cDNA (200 ng/µl in water) encoding RyR1 constructs, in some cases together with a plasmid (100 ng/µl) encoding rabbit $Ca_V1.1$ (GenBank number: M23919), labeled at its N terminus with enhanced cyan fluorescent protein (ECFP-$Ca_V1.1$; Papadopoulos et al., 2004). The primary myotubes were used for experimentation 1–2 d after injection and the R1R3 myotubes 3 d after injection.

tsA201 cells were propagated, in a humidified incubator with 5% (vol/vol) CO_2, in high-glucose DMEM supplemented with 10% (vol/vol) FBS and 2 mM glutamine. For experiments, the cells were plated at a density of 2×10^5 cells in 35-mm dishes (for FRET experiments), or 2×10^6 cells in 100-mm dishes for FPLC, and transfected 24 h later by using jetPRIME (Polyplus-transfection Inc.) with equimolar ECFP-RyR1$_{1:4300}$ and EYFP-RyR1$_{1:4300}$ (1 µg/35-mm dish each for FRET experiments) or with EYFP-RyR1$_{1:4300}$ only (10 µg/100-mm dish for FPLC) cDNA. Four hours after transfection, cells were removed from the dish by using Trypsin EDTA (Mediatech), split 1:2 into fresh medium, and replated into 35-mm culture dishes with glass-coverslip bottoms (MatTek) for FRET analysis or into 100-mm dishes for FPLC. Approximately 48 h after transfection, positively transfected cells were identified by the pattern of cyan and/or yellow fluorescence and used for FRET analysis or harvested for FPLC.

Confocal microscopy and quantification of $Ca_V1.1$ colocalization with RyR1 or RyR1$_{1:4300}$

Cells were superfused with Rodent Ringer's solution (mM: 146 NaCl, 5 KCl, 2 $CaCl_2$, 1 $MgCl_2$, and 10 HEPES, pH 7.4 with NaOH) and examined by using either a Zeiss LSM710 or an Olympus FluoView1000 (FV1000) laser-scanning microscope with a 40× or 63× oil immersion objective. For ECFP, excitation was 440 nm, and emission was recorded with a 465–495-nm bandpass. For EGFP, excitation was 488 nm, and emission was a 505-nm long pass. For EYFP, excitation was 514 nm (LSM710) or 515 nm (FV1000), and emission was a 530-nm long pass.

For the coexpression of ECFP-$Ca_V1.1$ with either EYFP-RyR1 or EYFP-RyR1$_{1:4300}$, colocalization was quantified for image subregions (see Eq. 1) by means of the Pearson correlation coefficient (PC):

$$PC = \frac{\sum_{i=1}^{n} \left(F_{ECFP,i} - \overline{F_{ECFP}} \right) \cdot \left(F_{EYFP,i} - \overline{F_{EYFP}} \right)}{\sqrt{\sum_{i=1}^{n} \left(F_{ECFP,i} - \overline{F_{ECFP}} \right)^2 \cdot \sum_{i=1}^{n} \left(F_{EYFP,i} - \overline{F_{EYFP}} \right)^2}}, \qquad (1)$$

where $F_{ECFP,i}$ and $F_{EYFP,i}$ are the background-corrected fluorescence intensities (F) measured for ECFP-$Ca_V1.1$ and for EYFP-RyR1 or EYFP-RyR1$_{1:4300}$, at the ith pixel, respectively. n is the total pixel number of the scan subregion, and $\overline{F_{ECFP}}$ and $\overline{F_{EYFP}}$ are the mean F values for that subregion. The background was calculated as the mean intensity within a region of interest in an adjacent, nontransfected myotube. For a transfected myotube, calculation was performed for one to three rectangular subregions ranging in area from 70 to 375 µm^2, corresponding to 4,000 to 21,000 pixel^2, respectively, with the calculated dimension of a single pixel being 133 × 133 nm. The PC for that myotube then represented the mean of all the subregions. Selection criteria for subregions to analyze were the presence of fluorescent foci of any type and, as possible, the absence of (auto-)fluorescent or precipitated material (as was often the case in perinuclear regions at the injected site). Identical calculations were then performed for the same subregions after shifting the ECFP scan laterally by four pixels relative to the EYFP scan, excluding the four rows of orphan pixels at either edge of the shifted images.

Characterization of RyR1$_{1:4300}$ mobility

To assess the mobility of diffusely distributed EYFP-RyR1$_{1:4300}$ expressed in dysgenic myotubes, an Olympus FV1000 confocal microscope was used to bleach the fluorescence within a 10-µm longitudinal segment of length by repeated scans at 515 nm with full laser power, which required ~5 s, followed by imaging of the bleached and adjacent regions at repeated intervals. To determine the stability of small foci of EGFP-RyR1$_{1:4300}$ after its expression in dyspedic myotubes, the cells were placed in a CO_2-independent medium (Gibco/Life Technologies) and contacted with a polished glass pipette having a tip diameter of ~5 µm and filled with (mM) 140 KCl, 5 $MgCl_2$, 10 HEPES, 10 EGTA, and 10 NaCl, pH 7.2, with NaOH. Repeated suction/pressure cycles applied to the pipette were

used to wash away diffusely distributed EGFP-RyR1$_{1:4300}$, followed by repeated imaging of the fluorescent foci.

Electrophysiological measurements

Macroscopic Ca^{2+} currents were measured with whole-cell clamping (Hamill et al., 1981) by using either a Dagan 3900 (Dagan) or PC-501A (Warner Instruments) amplifier, filtered at 2 kHz (four-pole Bessel) and digitized at 10 kHz by using a DigiData 1320A interface (Axon Instruments Inc.). Pipettes were fabricated from borosilicate glass and had resistances of ~2.0 MΩ when filled with intracellular solution containing (mM) 140 CsAsp, 5 MgCl$_2$, 10 Cs$_2$EGTA, and 10 HEPES, pH to 7.4 with CsOH. The external bath solution contained (mM) 10 CaCl$_2$, 145 tetraethylammonium-Cl, 0.003 tetrodotoxin (TTX), 0.1 N-benzyl-p-toluene sulphonamide (BTS), and 10 HEPES, pH to 7.4 with tetraethylammonium-OH. To isolate L-type currents, voltage was stepped from the holding potential (−80 mV) to −20 mV for 1 s to inactivate endogenous T-type current and then repolarized to −50 mV for 50 ms, depolarized to test potentials for 200 ms, repolarized to −50 mV for 100 ms, and then returned to the holding potential (Adams et al., 1990). Test currents were corrected for linear components of leak and capacitive current either by a –P/4 protocol or by digitally scaling and subtracting the mean of 11 control currents elicited by a hyperpolarizing step from −80 to −110 mV. Electronic compensation was used to reduce the effective series resistance (usually to <1 MΩ) and the time constant for charging the linear cell capacitance (usually to <0.5 ms). Cell capacitance was determined by integration of a transient from −80 to −70 mV and was used to normalize current amplitudes (pA/pF). Data were analyzed with the pCLAMP (Axon Instruments Inc.) and SigmaPlot (SPSS Inc.) software suites. Peak Ca^{2+} current–voltage (I-V) curves were fitted by using Eq. 2:

$$I = G_{max}(V\text{-}V_{rev})/\{1 + \exp[-(V\text{-}V_{1/2})/k_G]\}, \quad (2)$$

where I is the current for the test potential V, V_{rev} is the reversal potential, G_{max} is the maximum Ca^{2+} channel conductance, $V_{1/2}$ is the half-maximal activation potential, and k_G is the slope factor. The activation phase of the maximal Ca^{2+} current was fitted as shown in Eq. 3:

$$I(t) = A_{fast}[\exp(-t/\tau_{fast})] + A_{slow}[\exp(-t/\tau_{slow})] + C, \quad (3)$$

where I(t) is the current at time t after the depolarization, A_{fast} and A_{slow} are the steady-state current amplitudes of each component with their respective time constants of activation (τ_{fast}, and τ_{slow}), and C represents the steady-state current (Avila and Dirksen, 2000). To limit artifacts introduced by the declining phase of Q$_{on}$, the fitting procedure started at the zero-current level, 5–7 ms after the initiation of the test depolarization.

FPLC

48 h after transfection with EYFP-RyR1$_{1:4300}$, tsA201cells in 10-cm dishes were washed twice with PBS (Bio-Rad) and scraped free with 0.5 ml ice-cold homogenization buffer: 20 mM Tris, 50 mM KCl, pH 7.4, with one mini Protease Inhibitor tablet (Roche) per 10 ml. The scraped material was placed in a 1.5-ml Eppendorf tube, centrifuged 1 min at 10,000 g, homogenized with a conical pestle, and centrifuged for 1 h at 100,000 g. The supernatant was filtered at 0.2 µm, and a 0.5-ml aliquot was run on a Superose 6 10/300 GL column (GE Healthcare Life Sciences) at 0.5 ml/min, with the effluent collected in 0.25-ml fractions. Molecular weight standards run separately were 3 mg/ml apoferritin (Sigma), 5 mg/ml thyroglobulin (Sigma), and 1 mg/ml blue dextran 2000 (Sigma). In triplicate, 50 µl of each sample eluate fraction was blotted onto a 0.45-µm nitrocellulose membrane (Bio-Rad) with a Bio-Dot Microfiltration apparatus (Bio-Rad), where the membrane was wetted before sample application with Tris-buffered saline with Tween (TBS-T; 20 mM Tris, 500 mM NaCl and 0.05% [vol/vol] Tween 20), postblotted with an additional 50 µl TBS-T, removed from the apparatus, and washed quickly in 10 ml TBS-T. The membrane was exposed for 1 h at room temperature to blocking buffer (2.5% [wt/vol] nonfat dry milk in TBS-T), exposed overnight at 4°C to monoclonal antibody 34C (Developmental Hybridoma Studies Bank), diluted 1:500 in blocking buffer, washed at room temperature three times for 10 min in TBS-T, and exposed for 1 h to horseradish peroxidase-conjugated goat anti–mouse IgG. The immunoblots were developed by using the SuperSignal West Femto Maximum Sensitivity Substrate (ThermoFisher) and visualized on a Kodak imager.

FRET microscopy

FRET measurements were performed on R1R3 myotubes or tsA201 cells cotransfected with equimolar ECFP-RyR1$_{1:4300}$ and EYFP-RyR1$_{1:4300}$ and on R1R3 myotubes cotransfected with equimolar ECFP-RyR1 and EYFP-RyR1. FRET efficiency (E) was measured by enhanced donor (ECFP) emission after bleaching of the acceptor (EYFP): $E = \Delta C/C$, where ΔC is the increase in cyan emission intensity produced by bleaching EYFP and C is the cyan emission intensity after bleaching. In the case of the myotubes, emission intensities were measured only within the fluorescent puncta by using a thresholding procedure (Papadopoulos et al., 2004). To correct for inadvertent bleaching of ECFP that occurred during each confocal scan, two images were obtained before bleaching EYFP and two images afterward. More details on this correction and the thresholding procedure are provided in the Results section.

Freeze-fracture EM

For subsequent identification, large R1R3 myotubes expressing EYFP-RyR1 or EYFP-RyR1$_{1:4300}$ were imaged

Autonomous functions of RyR1's cytoplasmic domain | Polster et al.

with light microscopy and had their locations circumscribed by marking the glass, cover-slip bottom of the culture dish. The dishes were then washed twice with PBS and fixed in 2.5% glutaraldehyde in 0.1 M sodium cacodylate buffer (pH 7.4). Nonexpressing myotubes were then scraped away from the areas surrounding the previously identified myotubes, which were then infiltrated with 30% glycerol in H_2O at room temperature, freeze-fractured, shadowed with platinum at an angle of 45°, and replicated with carbon in a Balzers freeze-fracture unit (model BFA 400; Balzers S.P.A.; Paolini et al., 2004a; Takekura et al., 2004). The replicas were examined in a Philips 410 electron microscope (Philips Electron Optics) and the images digitally recorded with a Hamamatsu C4742-95 digital camera (Advanced Microscopy Techniques).

RESULTS

RyR1$_{1:4300}$ associates with SR–PM junctions only in myotubes expressing Ca$_V$1.1

Fig. 1 illustrates the subcellular distribution of RyR1 and that of its isolated cytoplasmic domain, RyR1$_{1:4300}$, expressed in various types of myotubes. The full-length construct, EYFP-RyR1, was concentrated in foci near the surface after expression in either dysgenic (Ca$_V$1.1-null) or dyspedic (RyR1-null) myotubes (Fig. 1 A). This is the pattern expected for junctional proteins in myotubes (Flucher et al., 1994), in which a large fraction of the junctions are dyadic associations between the SR and PM. Additionally, it is consistent with earlier results showing that the junctional targeting of RyR1 does not depend on the presence of Ca$_V$1.1 (Franzini-Armstrong et al., 1991). In contrast, the subcellular distribution of EYFP-RyR1$_{1:4300}$ depended on whether or not Ca$_V$1.1 was present (Fig. 1 B): EYFP-RyR1$_{1:4300}$ was diffusely distributed in dysgenic myotubes lacking Ca$_V$1.1, whereas in dyspedic myotubes it was predominantly present as fluorescent foci superimposed on a lower level of diffuse, background fluorescence, which varied from cell to cell. Although the data in Fig. 1 (A and B) are consistent with the hypothesis that EYFP-RyR1$_{1:4300}$ can only associate with SR–PM junctions containing Ca$_V$1.1, they do not exclude the possibility that the diffuse distribution of EYFP-RyR1$_{1:4300}$ in dysgenic myotubes resulted not from the absence of Ca$_V$1.1 but rather from the presence of endogenous RyR1, which could have prevented EYFP-RyR1$_{1:4300}$ from accessing the SR–PM junctions. Thus, we also expressed EYFP-RyR1$_{1:4300}$ in myotubes null for both Ca$_V$1.1 and RyR1 (Fig. 1 C). EYFP-RyR1$_{1:4300}$ was diffusely distributed despite the fact that SR–PM junctions containing junctional proteins are present in Ca$_V$1.1-RyR1 doubly null myotubes (Felder et al., 2002). Thus, the diffuse distribution in Ca$_V$1.1-RyR1 doubly null myotubes strengthens the conclusion that the truncated RyR1 can only associate with junctions containing Ca$_V$1.1.
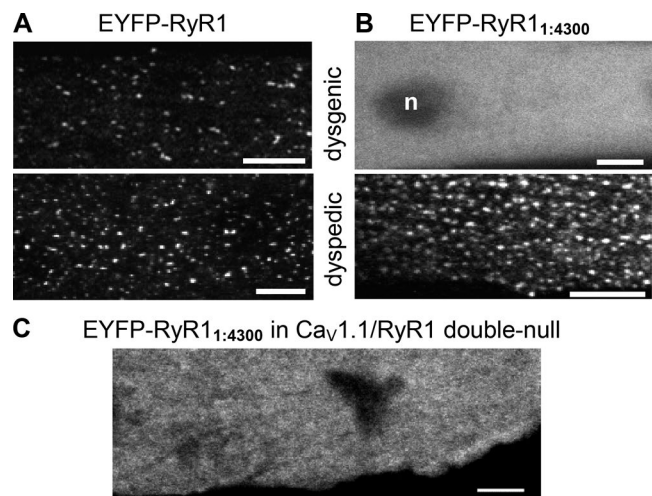

Figure 1. **Confocal scans near the surface of myotubes indicate that RyR1$_{1:4300}$ is able to localize at junctions between the sarcoplasmic reticulum and PM only when Ca$_V$1.1 is present. (A)** After expression in either dysgenic (Ca$_V$1.1-null) myotubes (top) or dyspedic (RyR1-null) myotubes (bottom), EYFP-RyR1 displayed a punctate distribution consistent with its targeting to SR–PM junctions. **(B)** In contrast, EYFP-RyR1$_{1:4300}$ was diffusely distributed in dysgenic myotubes (top, n indicates the nucleus) but was arrayed in discrete foci in dyspedic myotubes (bottom). **(C)** The lack of fluorescent puncta observed for EYFP-RyR1$_{1:4300}$ in dysgenic myotubes (shown in B, top) was not because the endogenous RyR1 occluded junctional binding sites because diffuse fluorescence was also observed when EYFP-RyR1$_{1:4300}$ was expressed in Ca$_V$1.1/RyR1 double-null myotubes. Bars, 5 µm.

To test directly the ability of RyR1$_{1:4300}$ to colocalize with Ca$_V$1.1-containing DHPRs, we coexpressed ECFP-Ca$_V$1.1 and EYFP-RyR1$_{1:4300}$ in dyspedic myotubes (Fig. 2 A). There was substantial overlap between ECFP-Ca$_V$1.1 and EYFP-RyR1$_{1:4300}$, as well as a few ECFP puncta (indicated in red) that were not associated with EYFP puncta (indicated in green) and a larger number of EYFP puncta that were not associated with ECFP puncta (the latter likely reflected the presence of EYFP-RyR1$_{1:4300}$ at SR–PM junctions containing endogenous, nonfluorescent Ca$_V$1.1). An appreciable, although incomplete, colocalization of ECFP-Ca$_V$1.1 and EYFP-RyR1$_{1:4300}$ coexpressed in dyspedic myotubes is also evident in a scatter plot of cyan versus yellow fluorescence of all the individual pixels within a representative image (Fig. 2 B, left). By comparison, a similar plot for ECFP-Ca$_V$1.1 and EYFP-RyR1 (Fig. 2 B, right) displayed less scatter in the relationship between ECFP and EYFP fluorescence. To quantify this comparison, we calculated PC values (Eq. 1), using both original images and images in which the cyan fluorescence image was shifted laterally by four pixels, as shown at high magnification in Fig. 2 C. The shift reveals that even if the foci in the original overlay (first row) are not perfectly superposed at the pixel level, virtually every
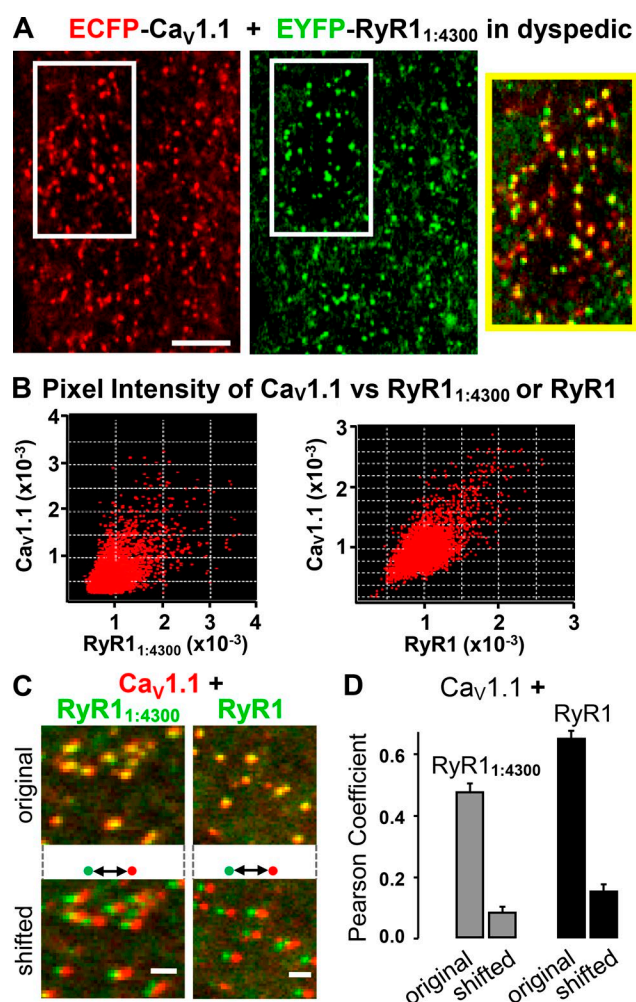
A **ECFP-Ca$_V$1.1 + EYFP-RyR1$_{1:4300}$ in dyspedic**

B Pixel Intensity of Ca$_V$1.1 vs RyR1$_{1:4300}$ or RyR1

C Ca$_V$1.1 +
RyR1$_{1:4300}$ RyR1

D Ca$_V$1.1 +

Figure 2. **RyR1$_{1:4300}$ colocalizes with Ca$_V$1.1. (A)** Coexpression of ECFP-Ca$_V$1.1 (red) and EYFP-RyR1$_{1:4300}$ (green) in dyspedic myotubes revealed extensive colocalization of the two proteins (yellow-bordered rectangle on the right illustrates the overlay of regions indicated by white rectangles), indicating that the subcellular localization of RyR1$_{1:4300}$ corresponds to junctions containing Ca$_V$1.1. Bar, 5 µm. **(B)** Representative pixel-by-pixel plots of cyan versus yellow fluorescence intensities for images of dyspedic myotubes expressing ECFP-Ca$_V$1.1 plus either EYFP-RyR1$_{1:4300}$ (left) or EYFP-RyR1 (right). Individual pixels are represented by a dot with ordinate and abscissa determined by the ECFP and EYFP fluorescence intensity, respectively, of that pixel. **(C)** Subregions of images obtained from dyspedic myotubes coexpressing ECFP-Ca$_V$1.1 and either EYFP-RyR1$_{1:4300}$ (left) or EYFP-RyR1 (right) before (original) and after the ECFP scan (red) was shifted rightward by four pixels (shifted) relative to the EYFP scan (green). Bars, 1 µm. **(D)** PC values (mean ± SEM) calculated for original and shifted images of dyspedic myotubes expressing ECFP-Ca$_V$1.1 and either EYFP-RyR1$_{1:4300}$ or EYFP-RyR1. Seven myotubes were analyzed for both construct combinations, with the PC for an individual myotube determined as the (mean) value for one to three subregions.

green patch in this example is associated with a red one. For the original images, the PC indicated substantial colocalization for Ca$_V$1.1 plus RyR1$_{1:4300}$ (0.47 ± 0.03), although less so than for Ca$_V$1.1 plus full-length RyR1
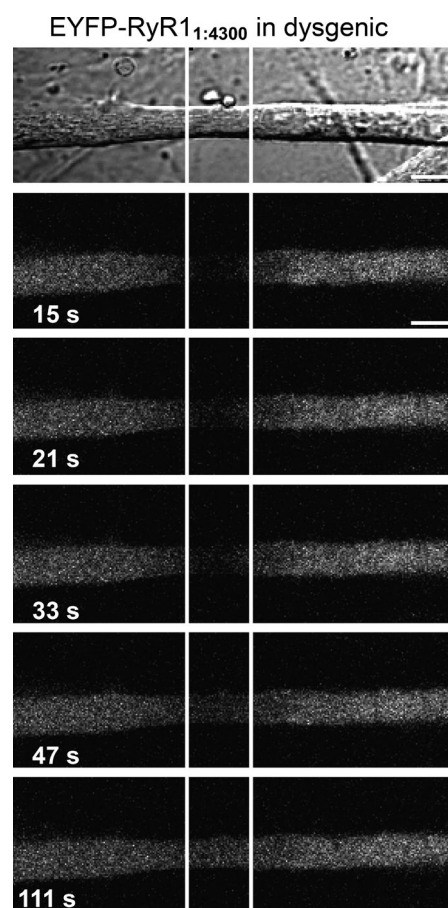
EYFP-RyR1$_{1:4300}$ in dysgenic

Figure 3. **EYFP-RyR1$_{1:4300}$ is mobile within the cytoplasm of dysgenic myotubes.** EYFP-RyR1$_{1:4300}$-expressing dysgenic myotubes were selected on the basis of being very long (compared with the width) and of having relatively uniform geometry along their length (top, transmitted light image). The fluorescence within a longitudinal segment near the center (vertical white lines) was bleached by repeated scanning for 5 s at 515 nm with maximum power, followed by imaging at repeated intervals (15, 21, 33, 47, and 111 s postbleach, in this example). Bars, 10 µm.

(0.65 ± 0.03). Laterally shifting the Ca$_V$1.1 image by four pixels caused the PC for RyR1$_{1:4300}$ to decrease to 0.08 ± 0.02, and that for RyR1 to 0.15 ± 0.02.

Mobility of RyR1$_{1:4300}$

To probe the mobility of diffusely distributed RyR1$_{1:4300}$ in dysgenic myotubes, we performed FRAP experiments, in which small areas were bleached by repeated, confocal scanning with laser intensities 20- to 100-fold higher than used for image acquisition. To approximate one-dimensional diffusion with an infinite source, we selected elongated dysgenic myotubes of approximately uniform geometry (Fig. 3). After 5 s of bleaching of EYFP-RyR1$_{1:4300}$, subsequent images displayed a slowly progressing recovery of fluorescence within the bleached segment. Thus, EYFP-RyR1$_{1:4300}$ was mobile in the cytoplasm of dysgenic myotubes.
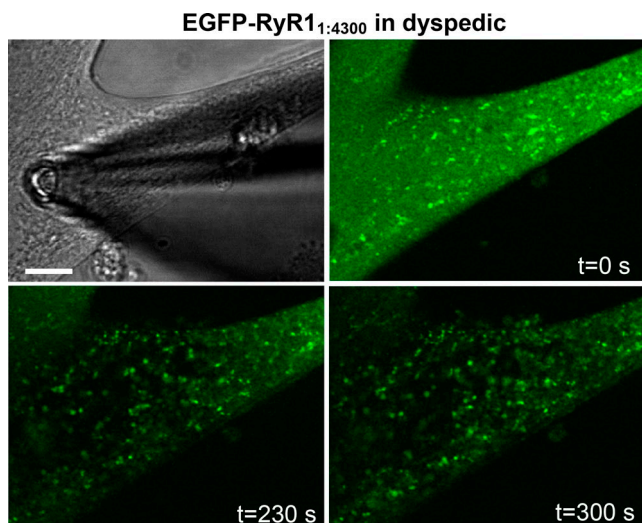
EGFP-RyR1$_{1:4300}$ in dyspedic

t=0 s

t=230 s

t=300 s

Figure 4. **EYFP-RyR1$_{1:4300}$ is stably bound at Ca$_V$1.1-containing junctions in dyspedic myotubes.** The transmitted light image (top left) shows a suction pipette pressed against the surface of a dyspedic myotube that had been transfected with EGFP-RyR1$_{1:4300}$. The fluorescence images acquired at the indicated times after the beginning of membrane rupture reveal the loss of diffuse green fluorescence and persistence of green fluorescence localized in foci. Bar, 10 µm.

To assess the rate of dissociation of RyR1$_{1:4300}$ from the punctate domains in dyspedic myotubes, we monitored the fluorescence of these domains before and after removal of mobile RyR1$_{1:4300}$ from the cytoplasm. Because the removal of the mobile pool by saponin permeabilization proved to be too slow, this was accomplished by means of suction via a large bore pipette (∼5-µm tip diameter). An example of such an experiment is illustrated in Fig. 4 for a dyspedic myotube transfected with EGFP-RyR1$_{1:4300}$. Immediately after the onset of suction, the cell displayed both diffuse and focal green fluorescence. Although cell movement made it difficult to follow the fate of individual foci over time, it was clear that, despite the removal of diffuse EGFP-RyR1$_{1:4300}$, bright fluorescent puncta were still present 5 min later. Similar results were obtained in 10 additional experiments. Thus, the association of RyR1$_{1:4300}$ with Ca$_V$1.1-containing PM–SR junctions appeared to have been relatively stable. Although not stringently comparable because of the methodological differences in the approaches, our results are in line with the FRAP measurements by Campiglio et al. (2013). The authors showed that there is no or only very little recovery in fluorescence upon bleaching GFP-α_{1S} in junctional foci, for an observation period of up to 5 min after photobleaching. Here, we demonstrate that in dyspedic myotubes the cytoplasmic RyR1 domain is, for a period of at least 5 min, as stably associated with the junctions as the membrane anchored Ca$_V$1.1.
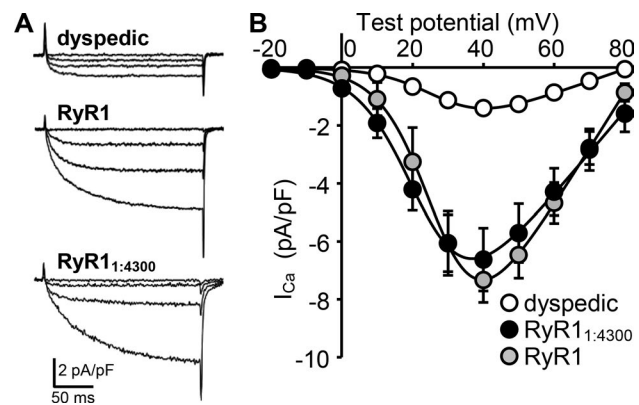

Figure 5. **Expression of EYFP-RyR1$_{1:4300}$ in dyspedic myotubes produces retrograde enhancement of Ca^{2+} current equivalent to that of full-length RyR1. (A)** Representative L-type Ca^{2+} currents (depolarizations to −20, 0, +20, and +40 mV) in a nontransfected dyspedic myotube and in dyspedic myotubes expressing either EYFP-RyR1 or EYFP-RyR1$_{1:4300}$. **(B)** Mean ± SEM peak I-V relationships for dyspedics ($n = 15$) and dyspedic myotubes expressing EYFP-RyR1 ($n = 11$) or EYFP-RyR1$_{1:4300}$ ($n = 11$). Smooth curves represent plots of Eq. 2.

EYFP-RyR1$_{1:4300}$ fully supports retrograde signaling

The localization of EYFP-RyR1$_{1:4300}$ at SR/PM junctions in dyspedic myotubes (Fig. 1) raised the question of whether this EYFP-RyR1$_{1:4300}$ could retrogradely signal to the DHPR in a manner like that of full-length RyR1 (Nakai et al., 1996; Avila and Dirksen, 2000). Specifically, in dyspedic myotubes, which lack RyR1 and thus lack retrograde signaling, Ca^{2+} currents via the DHPR are reduced in amplitude, and expression of full-length RyR1 causes an appreciable increase in current amplitude. Surprisingly, expression of the truncated RyR1 construct in dyspedic myotubes caused an increase in current amplitude very similar to that produced by the full-length construct (Fig. 5). In particular, maximal Ca^{2+} currents had a mean of 1.6 ± 0.2 ($n = 15$) in dyspedic myotubes, 7.4 ± 0.8 ($n = 11$) in dyspedic myotubes expressing EYFP-RyR1, and 6.7 ± 1.0 ($n = 11$) in dyspedic myotubes expressing EYFP-RyR1$_{1:4300}$ (calculated values of G$_{max}$ are given in Table 1). Fig. 5 also illustrates qualitatively a second aspect of retrograde signaling, which is the slowing of Ca^{2+} current activation (Avila and Dirksen, 2000), which we quantified by means of double-exponential fits (Eq. 3). As previously shown for full-length RyR1 (Avila and Dirksen, 2000), RyR1$_{1:4300}$ caused more than a doubling of both the fast and slow time constants of activation (Fig. 6). Moreover, the effects of RyR1$_{1:4300}$ on the time constants of activation were very similar to those of full-length RyR1. Thus, the truncated RyR1 not only binds at SR–PM junctions in the presence of Ca$_V$1.1, but also recapitulates the retrograde signaling of full-length RyR1 to the DHPR.
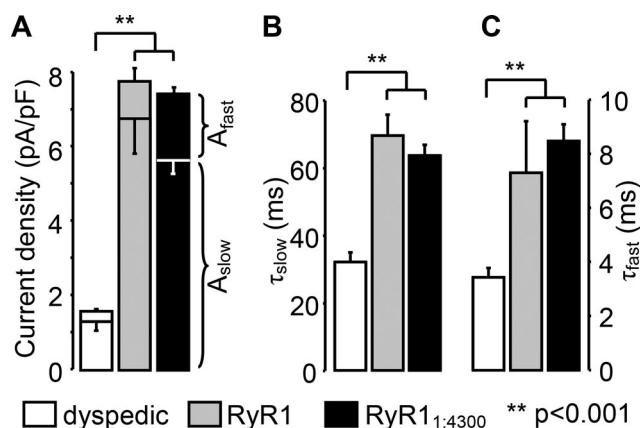
Figure 6. EYFP-RyR1$_{1:4300}$ causes a slowing of L-type current activation similar to that caused by EYFP-RyR1. (A–C) Maximal Ca^{2+} currents in dyspedic myotubes that were nontransfected (white bars, $n = 6$) or transfected with EYFP-RyR1 (gray bars, $n = 10$) or EYFP-RyR1$_{1:4300}$ (black bars, $n = 10$) were fitted as the sum of two exponential functions (Eq. 3), having amplitudes (mean ± SEM) A$_{slow}$ and A$_{fast}$ (A) and time constants τ$_{slow}$ (B) and τ$_{fast}$ (C).

Table 1. Conductance fits

Construct	G-V		
	G$_{max}$	**V$_{1/2}$**	**k$_G$**
	nS/nF	*mV*	*mV*
Dyspedic	42.3 ± 1.2 (15)	29.0 ± 1.5	7.8 ± 0.3
RyR1$_{1:4300}$	144.8 ± 4.8 (11)	23.0 ± 1.7	7.9 ± 0.3
RyR1	196.0 ± 6.2 (11)	27.8 ± 1.9	7.2 ± 0.2

Data are given as mean ± SEM, with the numbers in parentheses indicating the number of myotubes tested. Data were fit according to Eq. 2 (see Materials and methods).

Oligomerization of RyR1$_{1:4300}$

As just described, the effects of RyR1$_{1:4300}$ on Ca^{2+} currents via Ca$_V$1.1 were very similar to those of full-length RyR1, raising the question of whether these effects depended on oligomerization of RyR1$_{1:4300}$. As one approach for addressing this question, we analyzed EYFP-RyR1$_{1:4300}$ in the cytosolic lysate of transfected tsA201 cells by means of FPLC on a size-exclusion column. This analysis revealed that the majority of EYFP-RyR1$_{1:4300}$ in the lysate was monomeric (Fig. 7). Thus, the intermolecular interactions between the cytoplasmic domains, in the absence of the membrane-spanning and C-terminal domains, appeared to be too weak to cause EYFP-RyR1$_{1:4300}$ to be purely tetrameric in diluted cytosol. Nonetheless, eluate fractions corresponding to twice, or more, the mass of the monomer, contained a substantial amount of EYFP-RyR1$_{1:4300}$, indicating a tendency toward oligomerization, which might have been more extensive in intact cells in which the concentration of EYFP-RyR1$_{1:4300}$ would have been much greater.

The recent cryo-EM structures of full-length RyR1 (Efremov et al., 2015; Yan et al., 2015; Zalk et al., 2015) indicated that FRET could be used to obtain information about the oligomerization of RyR1$_{1:4300}$ within intact cells. Specifically, those structures revealed that the distance between N termini of adjacent monomers within an RyR1 tetramer is sufficiently small (<100 Å) that FRET should occur between ECFP and EYFP attached to the N termini of neighboring monomers. Thus, we expressed 1:1 mixtures of ECFP-RyR1 and EYFP-RyR1, or of ECFP-RyR1$_{1:4300}$ and EYFP-RyR1$_{1:4300}$, and measured FRET by means of enhanced donor (ECFP) fluorescence after acceptor (EYFP) photobleaching. As shown in Fig. 8, expression of these constructs in RyR1/RyR3-

null myotubes resulted in colocalized yellow and cyan fluorescent puncta indicative of SR–PM junctions. To measure the FRET occurring within these puncta, it was necessary to take into account the bleaching of ECFP that occurred during image acquisition. Thus, two scans were acquired before photo-bleaching EYFP and two afterward, which allowed us to extrapolate the cyan intensity just before bleaching (C$_R$) and just afterward (C$_F$). These provided two measures of FRET efficiency for each cell ([C3 − C$_F$]/C3 and [C$_R$ − C2]/C$_R$), whose mean was taken to provide a single value of FRET efficiency for that cell (Fig. 8, C and D). This analysis yielded a FRET efficiency of 8.6 ± 0.7% ($n = 20$) for full-length RyR1 and 3.6 ± 0.4% ($n = 12$) for RyR1$_{1:4300}$.

To determine whether the oligomerization of RyR1$_{1:4300}$ depended on its accumulation at SR–PM junctions, we also performed experiments on tsA201 cells where RyR1$_{1:4300}$ was observed to be diffusely distributed. The FRET efficiency of ECFP-RyR1$_{1:4300}$ plus EYFP-RyR1$_{1:4300}$ coexpressed in tsA201 cells was 3.2 ± 0.4 ($n = 15$), only slightly lower than that for RyR1$_{1:4300}$ at SR–PM junctions. This slightly lower efficiency may not be meaningful because mass transfection with cDNA (as used for the tsA201 cells) is likely to result in a larger cell-to-cell variability in the expression of ECFP-RyR1$_{1:4300}$ relative to EYFP-RyR1$_{1:4300}$ than the nuclear injection (used for myotubes). If this was the case, then the mean FRET efficiency would have been decreased by cells in which the copy number of ECFP-tagged species exceeded that of the EYFP-tagged species. Thus, it appears from the results of the FRET analysis that oligomerization occurs for RyR1$_{1:4300}$ both in the cytosol of intact tsA201 cells and accumulated at SR–PM junctions, but, compared with full-length RyR1, either is less complete or results in tetramers with a greater distance between the N termini of adjacent monomers.

In addition to using FRET to investigate the quaternary structure of RyR1$_{1:4300}$, we also used freeze-fracture EM to determine whether the expression of RyR1$_{1:4300}$ might alter the organization of DHPRs within the PM. Previous, freeze-fracture analyses of muscle cells showed that DHPRs are arranged at PM–SR junctions such that four of them fit just inside the corners of an ~30 × 30-nm square, although there

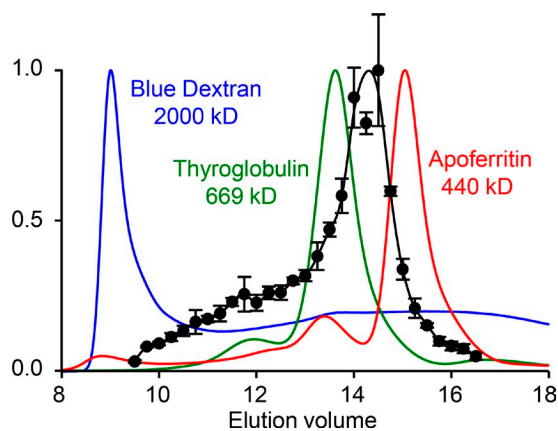Autonomous functions of RyR1's cytoplasmic domain | Polster et al.

Figure 7. FPLC indicates that RyR1$_{1:4300}$ in diluted cytosolic lysate of tsA201 cells is partially oligomerized but predominantly monomeric. Lysate from tsA201 cells transfected with EYFP-RyR1$_{1:4300}$ were subjected to FPLC on a Superose 6 10/300 GL column, with the content of EYFP-RyR1$_{1:4300}$ in 0.25-ml eluate fractions determined in triplicate by immunoblotting with monoclonal antibody 34C. The normalized immunostaining intensity is compared with the normalized 280-nm absorbance for the indicated standards. The position of the major immunostaining peak corresponds to that for the predicted mass of monomeric EYFP-RyR1$_{1:4300}$ (512.3 kD), but higher molecular mass oligomers were also present. Error bars represent mean ± SEM.

are also "incomplete tetrads" containing, e.g., three particles, in which one or more of the particles appear to have been deformed, to be present only as sheared-off stubs, or to be entirely absent (Franzini-Armstrong and Kish, 1995; Paolini et al., 2004b). Previous work also showed that tetrads are absent in dyspedic myotubes lacking RyR1 but are restored by transfection with cDNA for RyR1 (Protasi et al., 1998). Here we tested whether RyR1$_{1:4300}$ could similarly restore tetrads. For these experiments, we used R1R3 myotubes produced from a cell line of myoblasts null for both RyR1 and RyR3 in order to avoid the potentially confounding presence of RyR3, which is expressed at low levels in developing skeletal muscle (Bertocchini et al., 1997) and because the absence of fibroblasts makes these myotubes especially well-suited for freeze-fracture analysis. Fig. 9 illustrates representative freeze-fracture replicas of R1R3 myotubes that were not transfected (Fig. 9, A–C) or transfected with either EYFP-RyR1$_{1:4300}$ (Fig. 9, D–F) or with EYFP-RyR1 (Fig. 9, G–I). In cells of all three categories, regions of the PM likely to be forming junctions with the SR could be recognized by a slightly domed appearance and a clustering of large particles having the size (6.5 nm) expected for DHPRs (Takekura et al., 2004; Gach et al., 2008). In the images shown, the overlaid, 30 × 30-nm squares highlight areas in which three (yellow) or four particle (red) tetrads appeared to be present in the cells transfected with either EYFP-RyR1$_{1:4300}$ (Fig. 9, D–F) or EYFP-RyR1
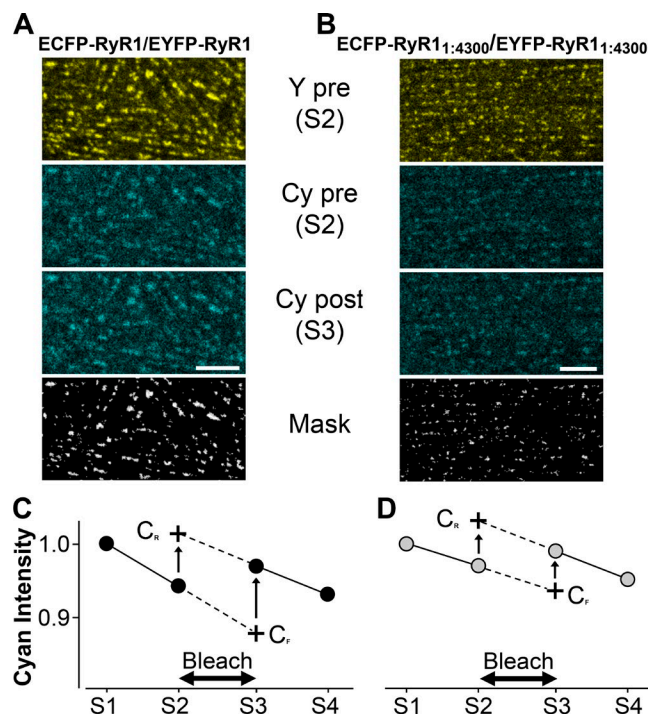

Figure 8. Intermolecular FRET indicates that RyR1$_{1:4300}$ oligomerizes at SR–PM junctions. (A and B) To measure FRET, four confocal scans (S1, S2, S3, and S4) were taken of RyR1/RyR3 double-null myotubes expressing 1:1 mixtures of cDNAs either encoding ECFP-RyR1 and EYFP-RyR1 (A) or encoding ECFP-RyR1$_{1:4300}$ and EYFP-RyR1$_{1:4300}$ (B), in which EYFP was photobleached between S2 and S3. Bars, 5 µm. To measure the cyan fluorescence intensities only within the fluorescent foci, a digital mask was produced by application of an adjustable threshold to the S1 image of EYFP such that all pixel values less than or equal to the threshold were set to zero (shown as black), and all values greater than the threshold (i.e., the majority of the yellow puncta) were set to one (shown as white). **(C and D)** Pixel intensities for cyan fluorescence were then measured only for mask pixels having the value one, yielding the mean cyan intensity (C1, C2, C3, and C4) for each of the four scans (S1 to S4), as shown in C and D for the cells illustrated in A and B, respectively (values normalized to C1). To account for the unavoidable bleaching of ECFP that occurred during each scan, extrapolated values of cyan fluorescence were calculated as $C_F = C2 × (C2/C1)$ and $C_R = C3 × (C3/C4)$, which provided two estimates of FRET efficiency for that cell: $[C3 − C_F]/C3$ and $[C_R − C2]/C_R$. The mean of these two estimates was taken as the FRET efficiency for the cell, which was 8.5% for the illustrated cell expressing ECFP-RyR1 and EYFP-RyR1 and 3.9% for the cell expressing ECFP-RyR1$_{1:4300}$ and EYFP-RyR1$_{1:4300}$.

(Fig. 9, G–I). In the nontransfected myotubes, cyan squares (Fig. 9, A and C) indicate regions in which there are clusters of three particles that resemble tetrads but perhaps fit less well within the squares than the particle groups illustrated for the transfected myotubes. However, to obtain an unbiased assessment, three expert morphologists were asked to quantify the prevalence of tetrads in unidentified images. The three individuals reported a significantly larger number of tetrads in the transfected myotubes than in the nontransfected
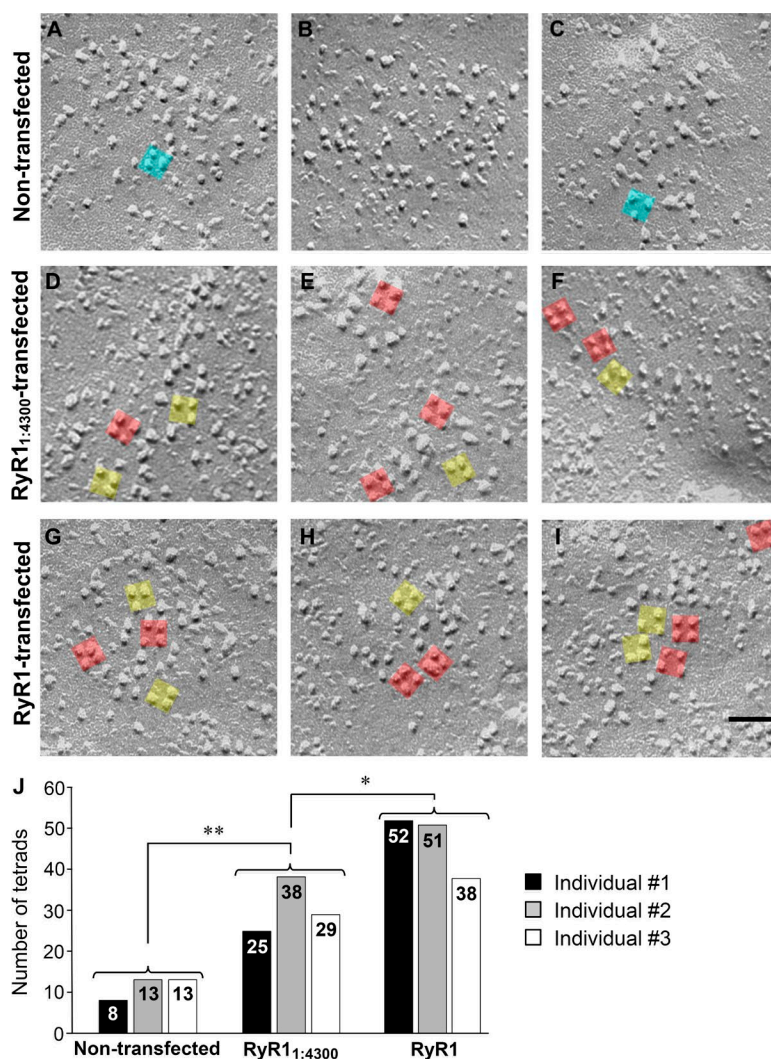
Figure 9. RyR1$_{1:4300}$ causes arrangement of DHPRs into tetrads. (A–I) Representative freeze-fracture replicas are shown of junctional regions of R1R3 myotubes (null for both RyR1 and RyR3) that were either nontransfected (A–C) or transfected with EYFP-RyR1$_{1:4300}$ (D–F) or with EYFP-RyR1 (G–I). Several clusters in the transfected myotubes (D–I) that appear to be partial (three-particle) or complete (four-particle) tetrads are indicated by yellow and red squares (30 × 30 nm), respectively; two groups resembling three-particle tetrads in the nontransfected myotubes are overlaid by cyan squares in A and C. Bar, 50 nm. **(J)** Numbers of three- or four-particle tetrads as determined by three individuals in 27 unidentified freeze-fracture images of R1R3 myotubes, of which nine were nontransfected, nine were transfected with EYFP-RyR1$_{1:4300}$, and nine were transfected with EYFP-RyR1. Each of the unidentified images was approximately twice the area of the images shown in A–I. The estimated number of junctional DHPRs ($\sim$6.5-nm particles in "domed" regions of the PM) was 557, 597, and 619 for nontransfected, EYFP-RyR1$_{1:4300}$-transfected, and EYFP-RyR1-transfected myotubes, respectively. Based on one-way ANOVA, the groups were significantly different: **, $P < 0.01$; *, $P < 0.02$.

myotubes (Fig. 9 J). Averaging for all three individuals, the number of apparent tetrads for full-length RyR1 was 4.1-fold that of control, whereas that for RyR1$_{1:4300}$ was lower but still substantial (2.7-fold). Thus, the freeze-fracture data support the conclusion that RyR1$_{1:4300}$ can form tetramers when expressed in myotubes.

DISCUSSION

Here, we have characterized the properties of a RyR1 cytoplasmic domain construct, RyR1$_{1:4300}$ that lacks residues 4,301–5,037, which contain the pore-forming segments and the cytosolic C-terminal domain of full-length RyR1. When expressed in dysgenic myotubes, null for Ca$_V$1.1, EYFP-RyR1$_{1:4300}$ was diffusely distributed, whereas it had a punctate distribution in dyspedic myotubes, null for RyR1 (Fig. 1 B). The punctate distribution in dyspedic myotubes is similar to that of PM–SR junctions (Flucher et al., 1994), which contain Ca$_V$1.1 in dyspedic myotubes but not in dysgenic myotubes. That the puncta indicated a junctional

association of RyR1$_{1:4300}$ with Ca$_V$1.1 was supported by the presence of colocalized foci of EYFP-RyR1$_{1:4300}$ and ECFP-Ca$_V$1.1 near the cell surface after their coexpression in dyspedic myotubes (Fig. 2). That some of the foci of EYFP-RyR1$_{1:4300}$ lacked corresponding foci of ECFP-Ca$_V$1.1 can be explained by the assumption that they represent association of EYFP-RyR1$_{1:4300}$ with junctions containing endogenous Ca$_V$1.1. The junctionally associated RyR1$_{1:4300}$ in dyspedic myotubes appeared to be immobile over a time period of at least a few minutes (Fig. 4), which contrasts with the mobility of the diffuse RyR1$_{1:4300}$ that was not bound at junctions (Fig. 3). Although one explanation for the absence of punctate fluorescence after expression of EYFP-RyR1$_{1:4300}$ in dysgenic myotubes (Fig. 1 B) is that these cells lack endogenous Ca$_V$1.1, an alternative is that the presence of endogenous RyR1 occluded access of the expressed EYFP-RyR1$_{1:4300}$ to a junctional protein having nothing to do with Ca$_V$1.1. Arguing against this latter possibility is that yellow foci were also absent after expression of EYFP-RyR1$_{1:4300}$ in myotubes null for both Ca$_V$1.1 and

RyR1 (Fig. 1 C). Although we did not directly test for the occurrence of SR/PM junctions in these cells, $Ca_V1.1$/RyR1 doubly null myotubes have been reported to contain such junctions (Felder et al., 2002). Thus, it seems likely that EYFP-RyR1$_{1:4300}$ binds to $Ca_V1.1$ or associated proteins whose presence, or conformation, in junctions depends on $Ca_V1.1$.

To an extent similar to that of full-length RyR1, expression of RyR1$_{1:4300}$ in dyspedic myotubes increased the amplitude, and decelerated activation kinetics, of the L-type current via $Ca_V1.1$ (Figs. 5 and 6). This result provides strong evidence that this isolated, cytoplasmic domain of RyR1 participates in many (or possibly all), of the protein–protein interactions that link full-length RyR1 to $Ca_V1.1$. Additionally, it confirms earlier work showing that activation of Ca^{2+} release via RyR1 is not involved in the retrograde effect on $Ca_V1.1$ channel function (Hurne et al., 2005). In that work it was shown that retrograde enhancement of Ca^{2+} current was produced by mutant RyR1 constructs (C4958S or C4961S) that did not release Ca^{2+} in response to either depolarization or application of caffeine. From these results, one could speculate that the retrograde signal depends only on static interactions between the RyR1 cytoplasmic domain and $Ca_V1.1$ (and/or closely associated junctional proteins). However, it is also possible that, despite being severed from the pore-forming domains, RyR1$_{1:4300}$ nonetheless undergoes conformational changes in response to $Ca_V1.1$ and that these could be involved in the retrograde enhancement of L-type current.

Truncation of RyR1 at residue 4,300 removes the pore-forming, transmembrane segments, as first proposed by Du et al. (2002) and now confirmed by cryo-EM (Efremov et al., 2015; Yan et al., 2015; Zalk et al., 2015). Additionally, this truncation eliminates the cytoplasmic C-terminal domain, which has been suggested to play a direct role in tetramerization (Stewart et al., 2003; Lee and Allen, 2007), and an interprotomer interaction between the EF-hand pair (residues 4,072–4,135) and the S2–S3 helical bundle, which is distal to 4,300 in the adjacent protomer (Zalk and Marks, 2017). Thus, one would expect tetramerization to be weaker for RyR1$_{1:4300}$ than for full-length RyR1. Consistent with this expectation, FPLC indicated that the majority of RyR1$_{1:4300}$ was monomeric in the cytosolic lysate of transfected tsA201 cells, with few, if any, tetramers present (Fig. 7). However, a nonnegligible fraction (∼25%) of RyR1$_{1:4300}$ in the lysate appeared to exist in complexes larger in size than the monomer, indicating the possibility that some interprotomer interactions were preserved in this truncated construct. Indeed, the cryo-EM structures indicate that this might be the case. Following the terminology of Zalk and Marks (2017), the N-terminal domain (NTD-A and NTD-B, residues 1–627), SPRY domains (628–1,656), bridging solenoid

(residues 1,658–3,613), and core solenoid (residues 3,667–4,253) are all present in RyR1$_{1:4300}$. These regions encompass several interprotomer contacts, including those between NTD-A and NTD-B (i.e., two contacts between adjacent protomers), NTD-A and the core solenoid, NTD-B and the bridging solenoid, and two regions of the bridging solenoid and the SPRY3 domain (Zalk and Marks, 2017).

Work that preceded the high-resolution cyro-EM studies provides direct evidence that interprotomer interactions are sufficient to support the formation of tetramers by N-terminal regions representing 10–20% of the full-length RyR. Specifically, tetramerization was shown by x-ray crystallography for RyR1 residues 1–559 (Tung et al., 2010) and by cross-linking for a region of RyR2 (residues 1–906) strongly conserved with RyR1 (Zissimopoulos et al., 2013). As described earlier, the interprotomer interactions did not appear sufficiently strong to maintain tetramers of RyR1$_{1:4300}$ in diluted lysate of tsA201 cells. However, intermolecular FRET (Fig. 8) and freeze-fracture EM (Fig. 9) indicated that RyR1$_{1:4300}$ was substantially oligomerized in intact cells. Moreover, some simple assumptions lead to the conclusion that a significant fraction of RyR1$_{1:4300}$ in myotubes is tetrameric. Two of these assumptions are (1) that full-length RyR1 is entirely tetrameric and (2) that PM–SR junctions contain comparable numbers of protomers of full-length or truncated RyR1 after transfection of myotubes null for endogenous RyRs. The first assumption seems reasonable, a priori, and the second receives experimental support from the quantitative similarities of L-type Ca^{2+} current after expression of full-length RyR1 or RyR1$_{1:4300}$ (Figs. 5 and 6). The final assumption is that the prevalence of DHPR tetrads provides a readout on the tetramerization of the RyR1 constructs. After correction for the number of "false tetrads" reported for nontransfected cells, the mean number of tetrads was 19.33 and 35.66 for RyR1$_{1:4300}$ and RyR1, respectively (Fig. 9 J). Thus, the assumptions above lead to the conclusion that 54% (19.33 of 35.66) of RyR1$_{1:4300}$ localized at junctions is in the form of tetramers.

With assumptions, it is also possible to calculate the prevalence of tetrameric RyR1$_{1:4300}$ from the efficiency of intramolecular FRET, which was 3.6% for ECFP-RyR1$_{1:4300}$ plus EYFP-RyR1$_{1:4300}$ and 8.6% for ECFP-RyR1 plus EYFP-RyR1 (Fig. 8). One fairly necessary assumption is that the ECFP- and EYFP-tagged monomers are expressed 1:1 and assemble with binomial statistics. If one then additionally assumes that full-length RyR1 at junctions is present only as tetramers and that RyR1$_{1:4300}$ is present as a mix of tetramers and monomers, then the measured FRET efficiency of 3.6% would imply that 42% of RyR1$_{1:4300}$ is tetrameric.

The preservation of the tetradic arrangement of DHPRs in freeze fractures depends on the strength of

association between the DHPRs and the underlying matrix of RyRs. In the case of full-length RyR1, this matrix is stabilized both by the membrane anchoring segments of individual RyRs and by the neighbor-neighbor interactions that organize RyR1 into a regular, two-dimensional lattice. It seems possible that the absence of these interactions for RyR1$_{1:4300}$ causes tetrads to be more prone to disruption during fixation and fracturing. Supposing this to be correct, and further supposing that all of RyR1$_{1:4300}$ in junctions is tetrameric, then the lower FRET efficiency compared with full-length RyR1 could be explained on the basis that the conformation of RyR1$_{1:4300}$ increases the distance between the N-terminal fluorescent proteins. If it is assumed that FRET can only occur between neighboring protomers (say with an efficiency of E%) within tetramers, then the FRET efficiency determined by enhanced donor emission after acceptor photobleaching would also be E for tetramers in which the content of ECFP- and EYFP-labeled protomers obeys the binomial probability distribution. Using the equation d = R$_o$[(1 − E)/E]$^{1/6}$ with R$_o$ = 4.9 nm for ECFP and EYFP (Patterson et al., 2000) yields calculated distances between neighboring N termini of 6.37 nm and 7.06 nm for RyR1 and RyR1$_{1:4300}$, respectively. This increased distance of 0.69 nm between neighboring N termini of RyR1$_{1:4300}$ does not seem to be overly large given that RyR1 tetramers (viewed from the cytoplasm) have a square outline ∼20 nm on a side (Yan et al., 2015). Furthermore, the RyR1 cytoplasmic domain seems easily capable of undergoing substantial conformational changes. In particular, treating cultured muscle cells with a high concentration of ryanodine caused the distance between adjacent DHPRs in tetrads to change by ∼2 nm (Paolini et al., 2004a).

In summary, we have shown that the ∼485-kD cytoplasmic domain of the C-terminally truncated RyR1 (RyR1$_{1:4300}$), although missing its SR membrane-spanning and cytoplasmic C-terminal domains, associates and functionally interacts with Ca$_V$1.1 at PM–SR junctions in living myotubes. The absence of the membrane-spanning and C-terminal domains destabilizes tetramerization such that most RyR1$_{1:4300}$ in diluted cytoplasm elutes as monomer on a size-exclusion FPLC column. However, both FRET measurements and freeze-fracture analysis indicate that a substantial fraction of RyR1$_{1:4300}$ is tetrameric in a cellular environment. Consequently, RyR1$_{1:4300}$ provides a valuable new tool for identifying the determinants that govern the interactions that structurally and functionally link Ca$_V$1.1 to RyR1. One important question is whether the junctional binding of RyR1$_{1:4300}$ observed in dyspedic myotubes can be recapitulated in fibroblastic cells by the expression of Ca$_V$1.1 and its auxiliary subunits, which is now made possible by the additional expression of Stac3 (Polster et al., 2015). If not, are additional junctional proteins necessary for

such binding to occur? Answers to such questions would provide significant new insight into the protein–protein interactions that are important for the communication between Ca$_V$1.1 and RyR1 in skeletal muscle.

REFERENCES

Adams, B.A., T. Tanabe, A. Mikami, S. Numa, and K.G. Beam. 1990. Intramembrane charge movement restored in dysgenic skeletal muscle by injection of dihydropyridine receptor cDNAs. *Nature.* 346:569–572. https://doi.org/10.1038/346569a0

Armstrong, C.M., F.M. Bezanilla, and P. Horowicz. 1972. Twitches in the presence of ethylene glycol bis(β-aminoethyl ether)-N,N′-tetracetic acid. *Biochim. Biophys. Acta.* 267:605–608. https://doi.org/10.1016/0005-2728(72)90194-6

Avila, G., and R.T. Dirksen. 2000. Functional impact of the ryanodine receptor on the skeletal muscle L-type Ca^{2+} channel. *J. Gen. Physiol.* 115:467–480. https://doi.org/10.1085/jgp.115.4.467

Beam, K.G., and C. Franzini-Armstrong. 1997. Functional and structural approaches to the study of excitation-contraction coupling. *Methods Cell Biol.* 52:283–306. https://doi.org/10.1016/S0091-679X(08)60384-2

Bertocchini, F., C.E. Ovitt, A. Conti, V. Barone, H.R. Schöler, R. Bottinelli, C. Reggiani, and V. Sorrentino. 1997. Requirement for the ryanodine receptor type 3 for efficient contraction in neonatal skeletal muscles. *EMBO J.* 16:6956–6963. https://doi.org/10.1093/emboj/16.23.6956

Block, B.A., T. Imagawa, K.P. Campbell, and C. Franzini-Armstrong. 1988. Structural evidence for direct interaction between the molecular components of the transverse tubule/sarcoplasmic reticulum junction in skeletal muscle. *J. Cell Biol.* 107:2587–2600. https://doi.org/10.1083/jcb.107.6.2587

Buck, E.D., H.T. Nguyen, I.N. Pessah, and P.D. Allen. 1997. Dyspedic mouse skeletal muscle expresses major elements of the triadic junction but lacks detectable ryanodine receptor protein and

304

Autonomous functions of RyR1's cytoplasmic domain | Polster et al.

function. *J. Biol. Chem.* 272:7360–7367. https://doi.org/10.1074/jbc.272.11.7360

Campiglio, M., V. Di Biase, P. Tuluc, and B.E. Flucher. 2013. Stable incorporation versus dynamic exchange of β subunits in a native Ca²⁺ channel complex. *J. Cell Sci.* 126:2092–2101. https://doi.org/10.1242/jcs.jcs124537

Dirksen, R.T., and K.G. Beam. 1999. Role of calcium permeation in dihydropyridine receptor function. Insights into channel gating and excitation-contraction coupling. *J. Gen. Physiol.* 114:393–403. https://doi.org/10.1085/jgp.114.3.393

Du, G.G., B. Sandhu, V.K. Khanna, X.H. Guo, and D.H. MacLennan. 2002. Topology of the Ca²⁺ release channel of skeletal muscle sarcoplasmic reticulum (RyR1). *Proc. Natl. Acad. Sci. USA.* 99:16725–16730. https://doi.org/10.1073/pnas.012688999

Efremov, R.G., A. Leitner, R. Aebersold, and S. Raunser. 2015. Architecture and conformational switch mechanism of the ryanodine receptor. *Nature.* 517:39–43. https://doi.org/10.1038/nature13916

Eltit, J.M., R.A. Bannister, O. Moua, F. Altamirano, P.M. Hopkins, I.N. Pessah, T.F. Molinski, J.R. López, K.G. Beam, and P.D. Allen. 2012. Malignant hyperthermia susceptibility arising from altered resting coupling between the skeletal muscle L-type Ca²⁺ channel and the type 1 ryanodine receptor. *Proc. Natl. Acad. Sci. USA.* 109:7923–7928. https://doi.org/10.1073/pnas.1119207109

Felder, E., F. Protasi, R. Hirsch, C. Franzini-Armstrong, and P.D. Allen. 2002. Morphology and molecular composition of sarcoplasmic reticulum surface junctions in the absence of DHPR and RyR in mouse skeletal muscle. *Biophys. J.* 82:3144–3149. https://doi.org/10.1016/S0006-3495(02)75656-7

Flucher, B.E., S.B. Andrews, and M.P. Daniels. 1994. Molecular organization of transverse tubule/sarcoplasmic reticulum junctions during development of excitation-contraction coupling in skeletal muscle. *Mol. Biol. Cell.* 5:1105–1118. https://doi.org/10.1091/mbc.5.10.1105

Franzini-Armstrong, C. 1970. Studies of the triad: I. Structure of the junction in frog twitch fibers. *J. Cell Biol.* 47:488–499. https://doi.org/10.1083/jcb.47.2.488

Franzini-Armstrong, C., and J.W. Kish. 1995. Alternate disposition of tetrads in peripheral couplings of skeletal muscle. *J. Muscle Res. Cell Motil.* 16:319–324. https://doi.org/10.1007/BF00121140

Franzini-Armstrong, C., M. Pincon-Raymond, and F. Rieger. 1991. Muscle fibers from dysgenic mouse in vivo lack a surface component of peripheral couplings. *Dev. Biol.* 146:364–376. https://doi.org/10.1016/0012-1606(91)90238-X

Gach, M.P., G. Cherednichenko, C. Haarmann, J.R. Lopez, K.G. Beam, I.N. Pessah, C. Franzini-Armstrong, and P.D. Allen. 2008. α₂δ₁ dihydropyridine receptor subunit is a critical element for excitation-coupled calcium entry but not for formation of tetrads in skeletal myotubes. *Biophys. J.* 94:3023–3034. https://doi.org/10.1529/biophysj.107.118893

Hamill, O.P., A. Marty, E. Neher, B. Sakmann, and F.J. Sigworth. 1981. Improved patch-clamp techniques for high-resolution current recording from cells and cell-free membrane patches. *Pflugers Arch.* 391:85–100. https://doi.org/10.1007/BF00656997

Hurne, A.M., J.J. O'Brien, D. Wingrove, G. Cherednichenko, P.D. Allen, K.G. Beam, and I.N. Pessah. 2005. Ryanodine receptor type 1 (RyR1) mutations C4958S and C4961S reveal excitation-coupled calcium entry (ECCE) is independent of sarcoplasmic reticulum store depletion. *J. Biol. Chem.* 280:36994–37004. https://doi.org/10.1074/jbc.M506441200

Lee, E.H., and P.D. Allen. 2007. Homo-dimerization of RyR1 C-terminus via charged residues in random coils or in an alpha-helix. *Exp. Mol. Med.* 39:594–602. https://doi.org/10.1038/emm.2007.65

Lorenzon, N.M., M. Grabner, N. Suda, and K.G. Beam. 2001. Structure and targeting of RyR1: Implications from fusion of green fluorescent protein at the amino-terminal. *Arch. Biochem. Biophys.* 388:13–17. https://doi.org/10.1006/abbi.2000.2263

Moore, R.A., H. Nguyen, J. Galceran, I.N. Pessah, and P.D. Allen. 1998. A transgenic myogenic cell line lacking ryanodine receptor protein for homologous expression studies: Reconstitution of Ry1R protein and function. *J. Cell Biol.* 140:843–851. https://doi.org/10.1083/jcb.140.4.843

Nakai, J., R.T. Dirksen, H.T. Nguyen, I.N. Pessah, K.G. Beam, and P.D. Allen. 1996. Enhanced dihydropyridine receptor channel activity in the presence of ryanodine receptor. *Nature.* 380:72–75. https://doi.org/10.1038/380072a0

Paolini, C., J.D. Fessenden, I.N. Pessah, and C. Franzini-Armstrong. 2004a. Evidence for conformational coupling between two calcium channels. *Proc. Natl. Acad. Sci. USA.* 101:12748–12752. https://doi.org/10.1073/pnas.0404836101

Paolini, C., F. Protasi, and C. Franzini-Armstrong. 2004b. The relative position of RyR feet and DHPR tetrads in skeletal muscle. *J. Mol. Biol.* 342:145–153. https://doi.org/10.1016/j.jmb.2004.07.035

Papadopoulos, S., V. Leuranguer, R.A. Bannister, and K.G. Beam. 2004. Mapping sites of potential proximity between the dihydropyridine receptor and RyR1 in muscle using a cyan fluorescent protein-yellow fluorescent protein tandem as a fluorescence resonance energy transfer probe. *J. Biol. Chem.* 279:44046–44056. https://doi.org/10.1074/jbc.M405317200

Patterson, G.H., D.W. Piston, and B.G. Barisas. 2000. Förster distances between green fluorescent protein pairs. *Anal. Biochem.* 284:438–440. https://doi.org/10.1006/abio.2000.4708

Polster, A., S. Perni, H. Bichraoui, and K.G. Beam. 2015. Stac adaptor proteins regulate trafficking and function of muscle and neuronal L-type Ca²⁺ channels. *Proc. Natl. Acad. Sci. USA.* 112:602–606. https://doi.org/10.1073/pnas.1423113112

Protasi, F., C. Franzini-Armstrong, and P.D. Allen. 1998. Role of ryanodine receptors in the assembly of calcium release units in skeletal muscle. *J. Cell Biol.* 140:831–842. https://doi.org/10.1083/jcb.140.4.831

Stewart, R., S. Zissimopoulos, and F.A. Lai. 2003. Oligomerization of the cardiac ryanodine receptor C-terminal tail. *Biochem. J.* 376:795–799. https://doi.org/10.1042/bj20030597

Takekura, H., C. Paolini, C. Franzini-Armstrong, G. Kugler, M. Grabner, and B.E. Flucher. 2004. Differential contribution of skeletal and cardiac II-III loop sequences to the assembly of dihydropyridine-receptor arrays in skeletal muscle. *Mol. Biol. Cell.* 15:5408–5419. https://doi.org/10.1091/mbc.E04-05-0414

Takeshima, H., S. Nishimura, T. Matsumoto, H. Ishida, K. Kangawa, N. Minamino, H. Matsuo, M. Ueda, M. Hanaoka, T. Hirose, et al. 1989. Primary structure and expression from complementary DNA of skeletal muscle ryanodine receptor. *Nature.* 339:439–445. https://doi.org/10.1038/339439a0

Tanabe, T., K.G. Beam, J.A. Powell, and S. Numa. 1988. Restoration of excitation-contraction coupling and slow calcium current in dysgenic muscle by dihydropyridine receptor complementary DNA. *Nature.* 336:134–139. https://doi.org/10.1038/336134a0

Tung, C.C., P.A. Lobo, L. Kimlicka, and F. Van Petegem. 2010. The amino-terminal disease hotspot of ryanodine receptors forms a cytoplasmic vestibule. *Nature.* 468:585–588. https://doi.org/10.1038/nature09471

Yan, Z., X. Bai, C. Yan, J. Wu, Z. Li, T. Xie, W. Peng, C. Yin, X. Li, S.H.W. Scheres, et al. 2015. Structure of the rabbit ryanodine receptor RyR1 at near-atomic resolution. *Nature.* 517:50–55. https://doi.org/10.1038/nature14063

Zalk, R., and A.R. Marks. 2017. Ca^{2+} Release Channels Join the 'Resolution Revolution'. *Trends Biochem. Sci.* 42:543–555. https://doi.org/10.1016/j.tibs.2017.04.005

Zalk, R., O.B. Clarke, A. des Georges, R.A. Grassucci, S. Reiken, F. Mancia, W.A. Hendrickson, J. Frank, and A.R. Marks. 2015. Structure of a mammalian ryanodine receptor. *Nature.* 517:44–49. https://doi.org/10.1038/nature13950

Zissimopoulos, S., C. Viero, M. Seidel, B. Cumbes, J. White, I. Cheung, R. Stewart, L.H. Jeyakumar, S. Fleischer, S. Mukherjee, et al. 2013. N-terminus oligomerization regulates the function of cardiac ryanodine receptors. *J. Cell Sci.* 126:5042–5051. https://doi.org/10.1242/jcs.133538

Autonomous functions of RyR1's cytoplasmic domain | Polster et al.